Chapter 7
Rocks and Minerals

The fundamental components of terrestrial planets, rocky moons, asteroids and meteoroids are rocks and minerals. Therefore, an understanding of rocks and minerals is essential to understanding rocky objects in any planetary system. In this chapter we review basic mineral and rock types that are common, to one extent or another, to all such objects, and how these minerals are altered by pressure and temperature and thus with depth into a planet. Starting in Sect. 7.6, we apply these concepts to the interior of the Earth in a manner that allows comparison with other planets in Chap. 9. We begin by making some basic distinctions concerning rocks and minerals.

7.1 Rocks

Rocks differ from minerals in that minerals are crystalline solids having a definite chemical composition (e.g., quartz (SiO_2)), and rocks are consolidated assemblages of minerals. Rocks can be classified as igneous, sedimentary, or metamorphic, as follows.

7.1.1 Igneous Rocks

Igneous rocks are those that solidified directly from molten rock, in the form of either magma or lava. *Magma* is molten rock below the planetary surface, whereas *lava* is magma that comes out onto the surface.

The sizes of crystal grains in igneous rocks depend on the rate of cooling. If the rock cools quickly then there is no time for large crystals to form, and the crystals are small or absent. If the rock cools slowly then the crystals are larger.

E.F. Milone and W.J.F. Wilson, *Solar System Astrophysics: Background Science and the Inner Solar System*, Astronomy and Astrophysics Library,
DOI 10.1007/978-1-4614-8848-4_7, © Springer Science+Business Media New York 2014

Igneous rocks are divided into three types, based on grain size:

1. *Extrusive, or volcanic, rocks* formed from lava. Being on the surface, they cooled quickly and therefore have a very fine grain or no grain structure. They are often porous (containing pores or pockets formed by the release of dissolved gases) and are often associated with volcanic out throws or lava flows.
2. *Intrusive rocks* formed from magma at shallow depths below the surface. Because they remained covered, they cooled more slowly, and have small to medium grain sizes.
3. *Plutonic rocks* formed from magma which remained deep below the surface. They cooled very slowly, over millions of years, and have a coarse grain structure and low porosity.

7.1.2 Sedimentary Rocks

Sedimentary rocks are formed after igneous and other rocks are eroded (weathered), carried away by wind or water, and deposited as sediments. If these sediments become overlain by other sediments, they can eventually be compressed to form rock.

Some examples of sedimentary rocks on the Earth are:

1. *Limestone*: Formed from calcium carbonate ($CaCO_3$) from plankton that died and settled onto the ocean floor. Limestone is the main constituent of the Rocky Mountains.
2. *Sandstone*: Formed from quartz (SiO_2) or feldspar sand grains that were transported by wind or water and became cemented together under pressure by materials such as silica, clays and calcite. Quartz and feldspar are discussed later in this chapter.
3. *Mudstone*: Formed from mud, composed primarily of clay minerals, that has been compacted into rock. If the mudstone is in thin layers (laminated) that can be split apart (fissile), it is referred to as *shale*.

7.1.3 Metamorphic Rocks

Metamorphic rocks are formed when sedimentary or igneous rocks are metamorphosed (changed) by high temperature and pressure, without melting.

Some examples of metamorphic rocks on the Earth are:

1. *Marble*: Formed from compression and heating of limestone or other carbonate rock. Recrystallization destroys the original, sedimentary carbonate structure to give a uniform structure of interlocking crystals.
2. *Quartzite*: Formed from compression and heating of quartz sandstone. The quartz grains, together with the cementing material, are recrystallized to form a dense, hard rock that fractures through the quartz grains, whereas sandstone fractures around the quartz grains.

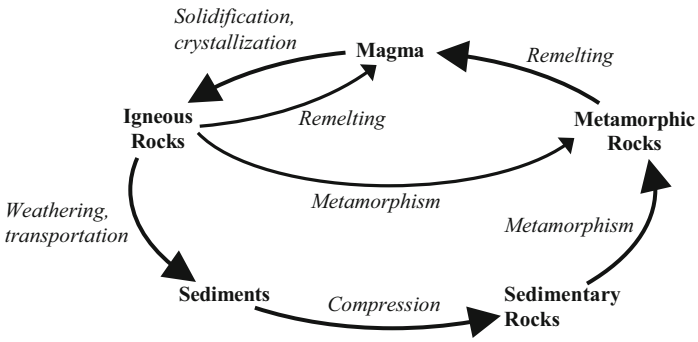

Fig. 7.1 The geochemical cycle

3. *Schist and gneiss*: Formed from compression of sedimentary rocks such as shales, or from igneous rocks. The layering is produced by shearing forces that align mica crystals and other platy minerals in planes perpendicular to the direction of compression.

The average composition of the Earth's crust is approximately 94 % igneous rock, 6 % sedimentary rock, and <1 % metamorphic rock.

7.1.4 The Geochemical Cycle

The *geochemical cycle* is shown schematically in Fig. 7.1. Heavy lines show the main cycle, in which magma solidifies to form igneous rocks that are subsequently weathered and compressed to form sedimentary rocks. These undergo metamorphism to produce metamorphic rocks, and the metamorphic rocks are remelted to form magma. Many other paths are also possible, two examples of which are shown by lighter lines.

7.2 Minerals

Each different mineral has its own chemical composition (e.g., $MgSiO_3$) and/or crystal structure (e.g., face-centered cubic) and/or crystal size (e.g., large, small, absent), etc.

7.2.1 Crystal Structure

There are many possible structures for crystals. We will describe two of these in detail here.

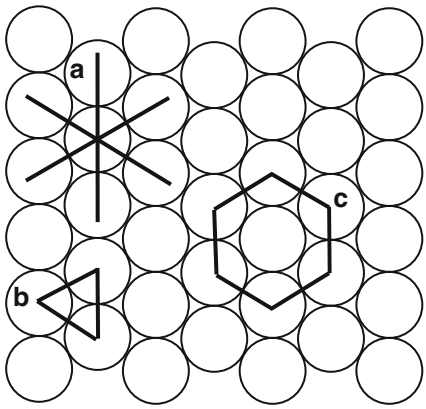

Fig. 7.2 A single layer of closely packed spheres

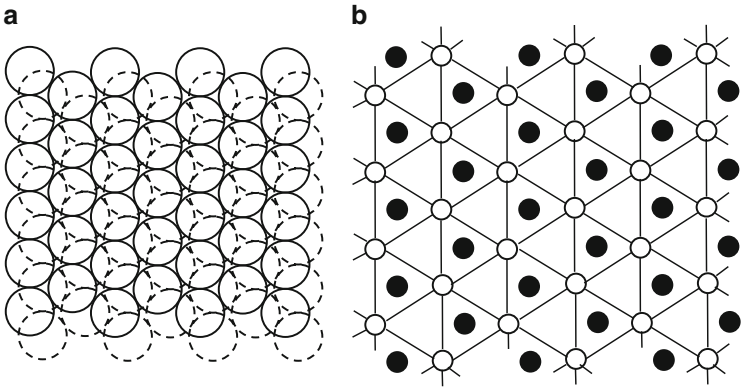

Fig. 7.3 Two layers of closely packed spheres with the upper layer resting as low as possible over the lower layer (see text)

We begin by packing spheres of equal size into a single layer in the densest possible manner, as shown in Fig. 7.2. Three properties of this close-packing arrangement are:

1. The spheres form a three-way grid (lines 120° apart), as indicated by the lines labeled "a" in Fig. 7.2.
2. Any three spheres in mutual contact form an equilateral triangle (e.g., the triangle labeled "b" in Fig. 7.2).
3. Every sphere has six equidistant neighbors touching it, forming a hexagon ("c" in Fig. 7.2).

If a second, identical, layer is stacked on top of this one, then the central planes of the two layers will be closest together when the second layer sits as low as it can over the first layer. This happens when the spheres in the upper layer lie over the holes (centers of the equilateral triangles) in the lower layer. Figure 7.3a shows the resulting arrangement. Here, solid circles represent the upper layer and dashed

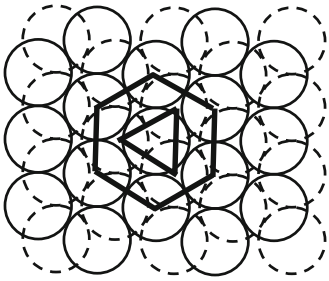

Fig. 7.4 A small section of Fig. 7.3a

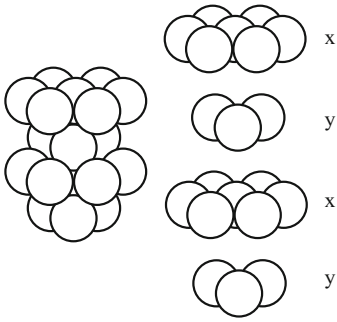

Fig. 7.5 Perspective (*left*) and exploded (*right*) views of four consecutive layers in hexagonal close packing (HCP)

circles represent the lower layer. Figure 7.3b shows a more open view (with a slightly expanded scale) which may make the arrangement clearer. Here, only the centers of the spheres are shown. Open circles indicate spheres in the upper layer, and filled circles indicate spheres in the lower layer.

A careful examination of Fig. 7.3 shows that some of the holes in the upper layer lie over *spheres* in the lower layer and others lie over *holes* in the lower layer. The fact that there are two types of holes in the upper layer means that there are now two different ways to stack a third (identical) layer on top of this one.

1. Stack the third layer so that its spheres are directly over the *spheres* in the layer two below it. If we continue stacking in this fashion, then the layers in Fig. 7.3 will alternate in an xyxyxy... pattern. The solid circles on the left side of Fig. 7.3 then represent ions in layers 1, 3, 5... and the dashed circles represent ions in layers 2, 4, 6....

   Figure 7.4 shows a portion of Fig. 7.3. Consider the hexagon of solid circles in Fig. 7.4 alternating with the triangle of dashed circles. The triangles are, of course, also parts of hexagons. Figure 7.5 shows (on the left) a three-dimensional view of four successive layers of this arrangement and (on the right) an exploded view of the same four layers.

   This method of stacking layers of spheres is called *hexagonal close packing* (HCP).
2. Stack the third layer so its spheres are over *holes* in *both* of the two layers below it. If we continue stacking in this fashion, then the spheres in any given layer are over the spheres in the layer *three* below, and the pattern of stacking that results is xyzxyzxyz....

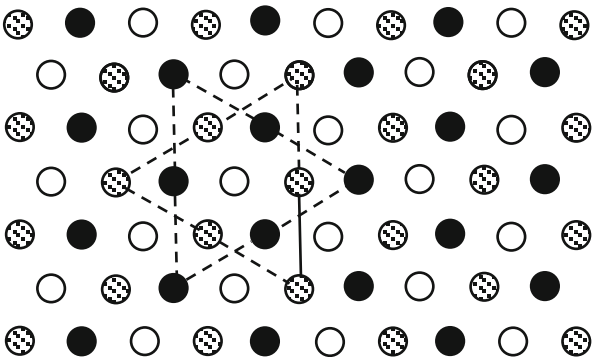

Fig. 7.6 A view through a crystal in which the layers are stacked xyzxyzxyz. . ., as explained in the text

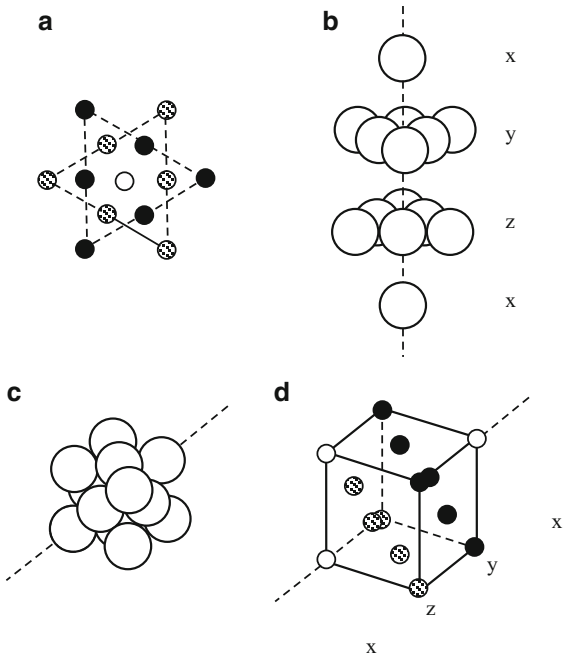

Fig. 7.7 Arrangement of layers and ions in cubic close packing (CCP), producing a face-centered cubic (FCC) crystal

Figure 7.6 shows a view through such a crystal (compare with the right-hand diagram in Fig. 7.3).

As we look down through the crystal, open circles represent layers 1, 4, 7,. . ., filled circles represent layers 2, 5, 8,. . ., and stippled circles represent layers 3, 6, 9,. . . The star-shaped arrangement shown in Fig. 7.6 is seen again in Fig. 7.7.

Other arrangements are also possible, such as xyzyxyzyx. . ., but these do not concern us here.

Figure 7.7a shows the star-shaped portion of Fig. 7.6. Figure 7.7b shows an exploded three-dimensional view of four successive layers in this portion. There are a total of 14 ions in these four layers. Figure 7.7c shows these same four layers pushed together as they exist in the crystal; and Fig. 7.7d shows schematically the locations of the 14 ions involved. Figure 7.7c, d have been rotated to the right and away from the viewer compared to Fig. 7.7b, as indicated by the dashed line (which is the same line in all three diagrams).

Figure 7.7c, d show that the 14 ions make up a cube. Eight ions form the corners of the cube, and the other six ions are located at the centers of the six faces. This xyzxyz . . . pattern is therefore referred to as *cubic close packing* (CCP), and forms a *face-centered cubic* (FCC) lattice.

Note that the layering formed by the top and bottom faces and the face-centered ions in the FCC pattern (Fig. 7.7c, d) is not the same as the layering we used to generate the pattern (Fig. 7.7a, b). The relationship between the two is shown by the arrangement of open, filled, and stippled circles in Fig. 7.7d, which correspond to the same symbols in the upper left-hand diagram, and in Fig. 7.6.

7.2.2 Crystal Density

If we pack steel balls in a box, then the balls in each layer are not directly affected by the balls in the layer two below. As a result, the layers are the same distance apart whichever arrangement (xyxyxy or xyzxyz) is used, and the overall density (g/cm^3 or kg/m^3) is the same for both HCP and CCP (or FCC).

However, ions of the same sign (+ or –) repel each other even if they are not physically touching. Therefore, an ion in a given layer is repelled more by the layer two below if the ion in the upper layer is over an ion in the lower layer (xyxyxy) than if it is over a hole in the lower layer (xyzxyz). As a result, a CCP (FCC) crystal has a greater density in kg/m^3 than an HCP crystal made of the same ions.

7.2.3 Interstitial Holes

When one layer is stacked on top of another to form a pair of layers in contact, holes (spaces) are created between the ions in one layer and the ions in the other layer. They are not the same as the "two-dimensional" holes discussed above, which are at the centers of the equilateral triangles *in* each layer. If we think of the midplanes of the layers as being located at $x = 0$ and $x = 1$, then for the close-packed layers discussed here the holes will be near $x = 1/2$. These holes between two layers are referred to as *interstitial holes*.

Interstitial holes have a three-dimensional structure, in that each hole is surrounded by a small, three-dimensional framework of ions. There are two types of interstitial holes, depending on the number of ions (shape of the framework) surrounding the hole:

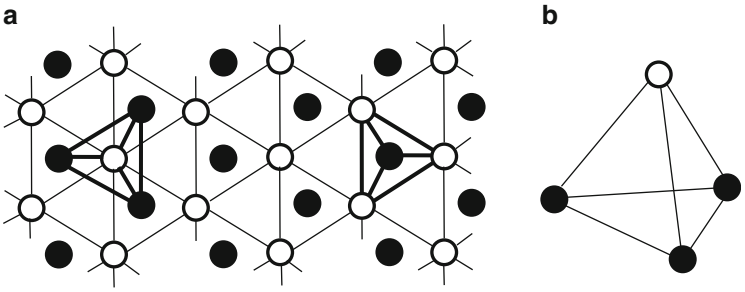

Fig. 7.8 Tetrahedral holes between adjacent layers of a crystal. *Open circles* represent ions in the upper layer and *filled circles* represent ions in the lower layer

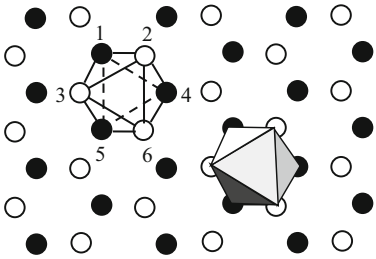

Fig. 7.9 Octahedral holes between adjacent layers of a crystal. *Open circles* represent ions in the upper layer and *filled circles* represent ions in the lower layer

7.2.3.1 Tetrahedral Holes

If an equilateral triangle of ions in the lower layer has an ion above it, then the hole between the two layers is surrounded by four ions, all in mutual contact. The hole is then at the center of a *tetrahedron* : a four-sided structure, each face of which is an equilateral triangle.

Two examples of tetrahedral holes are shown by heavy lines in Fig. 7.8a, with a three-dimensional view in Fig. 7.8b. (Remember that open and filled circles represent only the centers of the ions; the ions themselves are larger and in mutual contact.) The left-hand tetrahedron in Fig. 7.8a points out of the page, and the right-hand one points into the page.

7.2.3.2 Octahedral Holes

If the equilateral triangle in the lower layer does *not* have an ion over it in the layer above, then the hole between the layers is surrounded by *six* ions.

Two examples are shown in Fig. 7.9. In the left-hand example, the ions surrounding the hole are labeled from 1 to 6. The other example has been shaded to bring out the three-dimensional structure of the ions surrounding the hole more clearly.

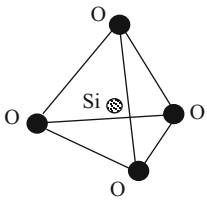

Fig. 7.10 Silicate tetrahedron. The silicon ion (*stippled circle*) occupies the tetrahedral hole at the center of the tetrahedral framework of four oxygen ions (*filled circles*)

Two of the ions in the lower layer (1 and 5) form a square with two in the upper layer (2 and 6). One other ion in the upper layer (3) and one in the lower layer (4) lie "above" and "below" the midpoint of the square, along its central axis.

As a result, the hole is at the center of an octahedron, an eight-sided figure made of two four-sided pyramids base-to-base.

7.2.4 The Silicate Tetrahedron

The crystals of silicate minerals (described below) can be regarded as stacked layers of oxygen ions, with silicon ions occupying a fraction of the tetrahedral sites and other metal ions occupying a fraction of the octahedral sites. The respective fractions of tetrahedral and octahedral sites occupied are different for different minerals.

The silicate tetrahedron (SiO_4) is shown in Fig. 7.10, and is the basic building block of almost all silicate minerals. (In the case of stishovite, perovskite and the post-perovskite phase, discussed below, the basic building block is a silicate octahedron.)

The valence of silicon is +4 and that of oxygen is –2, so the valence of SiO_4 is $4 + 4(-2) = -4$. Each SiO_4 therefore bonds easily with other ions, usually those of silicon or metals.

7.2.5 Mineral Names

Mineral names are somewhat arbitrary, because:

1. Minerals with the same crystal structure but different chemical compositions can have the same name. This happens because certain types of ions (e.g., magnesium and iron) are so similar to each other in size and chemical properties that one can replace the other in the octahedral sites with no change to the crystal structure.

   An example is olivine, a silicate mineral in which each occupied octahedral site contains an ion of either magnesium (Mg) or iron (Fe). If all such sites are occupied by Mg, then the mineral is called *forsterite* (Mg_2SiO_4), and if all are occupied by iron then the mineral is called *fayalite* (Fe_2SiO_4).

   However, these are simply end-members of a continuous series of possible compositions, and the chemical symbol for olivine is often given as

Table 7.1 Mean composition of the Earth's crust

Element	Symbol	Weight %	Atom %
Oxygen	O	46.60	60.5
Silicon	Si	27.72	20.5
Aluminum	Al	8.13	6.2
Iron	Fe	5.00	1.9
Calcium	Ca	3.63	1.9
Sodium	Na	2.83	2.5
Potassium	K	2.59	1.8
Magnesium	Mg	2.09	1.4
Titanium	Ti	0.44	
Hydrogen	H	0.14	
Phosphorus	P	0.12	
		99.29	

$(Mg_{(1-x)}Fex)_2\ SiO_4$, where x can have any value from 0 to 1. For example, $(Mg_{0\ 9}Fe_{0.1})_2SiO_4$ has 90 % of the sites occupied by magnesium and 10 % by iron. All these possible compositions are included in the name olivine.

Olivine is described more fully in Sect. 7.2.8.4.

2. Minerals with the *same* chemical composition can exist in different *phases* (different crystal lattices) and these can have different names.

   Olivine and silicate spinel (hereafter referred to simply as "spinel") provide an example. Both have the chemical symbol Mg_2SiO_4 (or Fe_2SiO_4, etc), but they differ in crystal structure: in olivine the oxygen ions are arranged in an HCP lattice and in spinel they are arranged in a CCP (or FCC) lattice.

   Spinel is a high-pressure phase of olivine. Olivine is common in the Earth's upper mantle, but deeper in the mantle where pressures are higher it undergoes a *phase transition* to the more closely packed crystal structure of spinel. Spinel therefore has the same chemical symbol as olivine, but is about 10 % denser. Spinel is discussed again in Sects. 7.2.8.4 and 7.4.2.

   A more familiar example of a substance changing name when it undergoes a phase transition is, of course, water changing to ice.

3. Some minerals have different names even though they have the same chemical composition *and* crystal structure, because they differ in crystal size or some other characteristic.

7.2.6 Composition of the Earth's Crust

The mean chemical composition of the Earth's crust, excluding some trace constituents, is given in Table 7.1.

That is, oxygen atoms make up 60.5 % of all atoms in the crust, but, because oxygen atoms are lighter than all of the others listed except hydrogen, they make up only 46.60 % of the mass or weight of the crust.

Oxygen and silicon together make up 74 % of the weight of the crust, or 81 % of the atoms. It is therefore clear that the most common minerals will be those involving oxygen and silicon: *the silicates*.

7.2.7 Oxygen-to-Silicon Ratio in Chemical Symbols

The basic crystal unit of most silicate minerals is the SiO_4 tetrahedron. If the tetrahedra are isolated from each other (i.e., they are not linked by sharing oxygen atoms), then the mineral will contain four oxygen atoms for every silicon atom and the chemical symbol will contain SiO_4, e.g., olivine, Mg_2SiO_4.

However, if some oxygen atoms are shared between adjacent tetrahedra (i.e., the tetrahedra are linked), then on average there are fewer oxygen atoms per silicon atom in the mineral. This sharing changes the chemical symbol, even though the basic crystal unit is still the SiO_4 tetrahedron; e.g., pyroxene, $MgSiO_3$; quartz, SiO_2.

7.2.8 Oxygen-to-Metal Ratio and the Classification of Silicate Minerals

One way to classify silicate minerals is by their oxygen-to-metal ratio.

The most common metals in silicate minerals are silicon, magnesium, iron, calcium, potassium, and sodium, but others are also possible.

The most common ratios are, in order of decreasing oxygen abundance (or increasing metal abundance):

$$\text{oxygen : metal} = 2{:}1 \;\; 8{:}5 \;\; 3{:}2 \text{ and } 4{:}3$$

7.2.8.1 2:1 Ratio: Silica (SiO_2)

Silica has different mineral names, depending on the crystal structure. Two examples are quartz and stishovite.

Quartz is a framework silicate: not all oxygen ions in the close-packing arrangements discussed above are actually present, and the remaining tetrahedra form a framework.

Figure 7.11 shows a single layer of linked tetrahedra in a quartz crystal. Large circles represent oxygen ions, and small circles represent silicon ions (dashed if hidden below an oxygen ion). The bases of the tetrahedra share oxygen ions to form a repeating pattern of hexagons, while the tetrahedra themselves point alternately up and down around each hexagon.

The upward-pointing tetrahedra in this layer share their oxygen ions with the downward-pointing tetrahedra in the next layer.

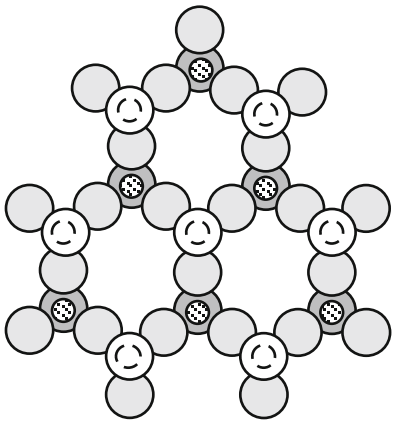

Fig. 7.11 A single layer of linked tetrahedra in a quartz crystal

The SiO_4 tetrahedra therefore link to form a three-dimensional framework in which each tetrahedron shares all four oxygen ions with its neighbors. The result is that, on average, there are two oxygen ions for every silicon ion, and the chemical symbol for silica is SiO_2, even though it is made up of linked SiO_4 tetrahedra (or linked SiO_6 octahedra).

Stishovite is a high-pressure (~20 GPa, where 1 GPa = 1 gigapascal = 10^9 Pa = 10 kbar) phase of quartz, made up of SiO_6 octahedra. The oxygen ions are shared between adjacent octahedra so that on average there are again two oxygen ions for every silicon ion, and the chemical symbol is still SiO_2.

7.2.8.2 8:5 Ratio: Feldspar Group

$M_2AlSi_2O_8$, where M_2 = two metal ions. One of the metal atoms in the chemical symbol is potassium, K, sodium, Na, or calcium, Ca, and the other is aluminum, Al, or silicon, Si. Three examples of feldspars are:

$$\begin{aligned} &\text{Orthoclase feldspar}: && KAlSi_3O_8 \\ &\text{Plagioclase feldspar}: && \begin{cases} NaAlSi_3O_8 \text{ (albite)} \\ CaAl_2Si_2O_8 \text{ (anorthite)} \end{cases} \end{aligned}$$

Feldspars are framework silicates like quartz. For example, in orthoclase the Al^{3+} replaces one of every four Si^{4+} in the tetrahedral sites in quartz, and the charge imbalance is compensated by introducing K^+ ions into octahedral sites.

7.2.8.3 3:2 Ratio: Pyroxene Group

$M_2Si_2O_6$, where M_2 = two metal ions. The metal atoms are commonly Ca, Mg, or Fe, or less commonly K, Al, Ti, or Na.

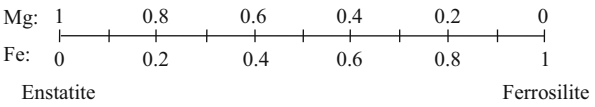

Fig. 7.12 Enstatite–ferrosilite series

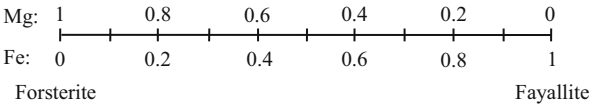

Fig. 7.13 Forsterite-fayalite series

Two examples of pyroxenes are enstatite, $MgSiO_3$ (equivalent to $Mg_2Si_2O_6$) and diopside, $CaMgSi_2O_6$.

As illustrated in Fig. 7.12, enstatite forms one end-member of a continuous series of possible compositions with ferrosilite, $FeSiO_3$, in which iron replaces the magnesium of the enstatite. The enstatite–ferrosilite series is referred to as (Mg,Fe)SiO_3. For example, the pyroxenes in the upper mantle have a composition near $(Mg_{0.9}Fe_{0.1})SiO_3$, which means that 90 % of the available spaces are filled by magnesium ions and 10 % by iron ions.

The $MgSiO_3$–$FeSiO_3$ series is referred to as *orthopyroxene,* and the $CaMgSi_2O_6$–$CaFeSi_2O_6$ series as *clinopyroxene*.

The pyroxenes are chain silicates: each tetrahedron shares a basal oxygen ion with the next to form a zigzagging chain stretching along the *c* direction. Because of the shared O ions, counting along a chain produces a sequence of one Si, three O, one Si, three O, etc.; so the silicate portion of the chemical symbol is SiO_3. Parallel chains form planes parallel to the *b,c* plane, and adjacent planes are separated (and bonded together) in the *a*-direction by the positive metal cations. All tetrahedra in a given chain have their apices pointing in the same direction, either upward or downward relative to the *b,c* plane. If the apices of one chain point "up," then those of the adjacent chains in both the *a* and *b* directions point down, with chains alternating in this fashion through the crystal.

Phase transitions in pyroxene at high pressures can produce garnet, perovskite, and the post-perovskite phase (i.e., a phase at a higher pressure than perovskite), described in Sects. 7.4.1.2, 7.4.1.4, and 7.4.1.5, respectively. These also have an oxygen:metal ratio of 3:2, and also have a range of compositions.

7.2.8.4 4:3 Ratio: Olivine and Spinel

M_2SiO_4, where M_2 = two metal ions (magnesium or iron). *Olivine* has a continuous range of compositions, referred to as $(Mg, Fe)_2SiO_4$, in which forsterite, Mg_2SiO_4, and fayalite, Fe_2SiO_4, are the two end-members. The series is illustrated in Fig. 7.13.

In olivine, the oxygen ions form an HCP lattice in which the SiO_4 tetrahedra are isolated from each other (that is, they do not share oxygen ions). The metal ions

(Mg or Fe) occupy octahedral sites between the tetrahedra and bond the silicate tetrahedra together in the *x, y* and *z* directions.

Spinel is a high-pressure phase of olivine, formed at pressures >12 GPa.

Olivine and spinel are described again in Sect. 7.4.2.

7.3 Mineral Content of Igneous Rocks

Table 7.2 lists the mineral content of igneous rocks.

In Table 7.2 we note the following:

1. The *amphibole* group consists of chain-type silicate minerals in which every second SiO_4 tetrahedron in a chain shares an oxygen ion with a tetrahedron in an adjacent chain, forming a double-chain structure. Adjacent double chains in amphibole are bonded together by positively charged ions, as is the case with the single chains of the pyroxenes.

2. *Pegmatite* is an uncommon rock that contains uranium, thorium, and other elements with unusual ion radii. These are the last to enter minerals in a solidifying magma, and therefore become concentrated in the crust.

3. *Eclogite* is obtainable by phase transitions from basalt (e.g., through subduction of basaltic crust). Eclogite may be one of the rock types making up the mantle.

4. *Pyrolite* (not listed in Table 7.2) is defined as any substance which can produce basaltic magma through partial melting, leaving behind dunite and peridotite as a result. Pyrolite in this picture is regarded as a single source material for both the basalt in the crust and the dunite and peridotite in the upper mantle, and is therefore itself an important constituent of the upper mantle.

   Pyrolite is a "fictitious" rock, in that it is defined in terms of what it does, leaving its actual mineral content to be determined. It seems to be composed of 2/3 olivine and 1/3 pyroxene, plus perhaps garnet.

5. *Serpentinite* (not listed in Table 7.2) is composed mainly of olivine and pyroxene combined with water. The water lowers the melting point significantly. Serpentinite is mentioned here only to show that the presence of water complicates the description of melting or crystallization of rocks in the Earth's upper mantle.

Table 7.2 Mineral content of igneous rocks

Density (g/cm)	Plutonic rock	Volcanic rock	Principal mineral content
	Pegmatite		Quartz, feldspar
2.7	Granite	Rhyolite	Quartz, feldspar
	Diorite	Andesite	Feldspar, amphibole
3.0	Gabbro	Diabase, basalt	Feldspar, pyroxene
	Peridotite		Pyroxene, olivine
3.5	Dunite		Olivine
	Eclogite		Pyroxene, garnet

Table 7.3 Felsic/mafic classification

Plutonic rock	Volcanic rock	Felsic/mafic	Acidity
Granite	Rhyolite	Felsic	Acidic
Diorite	Andesite	Intermediate	
Gabbro	Diabase, basalt	Mafic	Basic
Dunite, eclogite		Ultramafic	Ultrabasic

7.3.1 Classification of Rocks by Mineral Content

Rocks may be classified according to their feldspar, silica, magnesium, and iron content.

Granite and rhyolite are silica-rich, as shown by the fact that quartz is one of the principal minerals in each one (see Table 7.2). They are also rich in feldspar, so they have a relatively high content of potassium and sodium. Such rocks are classified as *felsic* because of their high *fel*dspar and *s*ilica content. They are also more *acidic* than basalt or dunite.

Gabbro and basalt contain less silica and more magnesium, iron, and calcium than felsic rocks, and are classified as *mafic* rocks, from the words *ma*gnesium and *f*erri*c*. They are *basic*, rather than acidic.

Rocks such as dunite and eclogite, which have an even higher magnesium and iron content and are even more basic, are often referred to as *ultramafic* or *ultrabasic*.

These classifications are shown in Table 7.3.

7.4 Phase Transitions

A phase of a mineral is a particular crystal structure for that mineral.

As pressure increases with depth into the mantle, minerals undergo phase transitions in which the atoms (ions) are rearranged into a different crystal structure; for example:

$$Mg_2SiO_4 \text{ olivine} \rightarrow Mg_2SiO_4 \text{ spinel},$$

where the HCP lattice of oxygen ions in the olivine phase is transformed to the denser CCP lattice in the spinel phase.

This rearrangement can also involve one crystal structure separating into two crystal structures (i.e., the original mineral separates into two minerals) or two crystal structures merging into one (two minerals merging into a single mineral); for example,

$$Mg_2SiO_4 \text{ spinel} \rightarrow MgSiO_3 \text{ perovskite} + MgO \text{ periclase}$$

MgO has the same crystal structure as NaCl (table salt), as described in Sect. 7.4.1.4.

7.4.1 Phase Transitions of Pyroxene, $MgSiO_3$

7.4.1.1 Pyroxene

This is the low-pressure phase, found on a planet's surface and in the crust, e.g., enstatite, $MgSiO_3$.

The crystal structure of enstatite consists of chains of corner-sharing silicate tetrahedra. Because of the sharing of oxygen ions there are, on average, three oxygen ions (valence –2) for each silicon ion (valence +4), so the valence of each SiO_3 unit (one silicon ion plus the base of a tetrahedron) is $3 \times (-2) + 4 = -2$. The valence of Mg and Fe is +2, so on average there is one Mg or Fe ion for each SiO_3 unit, giving the chemical symbol $(Mg,Fe)SiO_3$.

As described in Sect. 7.2.8.3, pyroxene has a variety of compositions. For example, $MgSiO_3$ enstatite forms a continuous series with $FeSiO_3$ ferrosilite by progressive replacement of Mg ions with Fe ions; or every second Mg ion in $MgSiO_3$ enstatite can be replaced by a calcium (Ca) ion, forming $CaMgSi_2O_6$ diopside.

7.4.1.2 Garnet

Pyroxene undergoes a phase transition to silicate garnet, $Mg_4Si_4O_{12}$, at about 17–19 GPa pressure and $T > 2{,}000$ K, as shown in Fig. 7.17.

During the phase transition, the silicate tetrahedra change from corner-sharing chains (pyroxene, silicate unit = SiO_3) to isolated tetrahedra (garnet, silicate unit = SiO_4). In the process, one silicon ion is "released" from a tetrahedron, producing five metal ions for every three silicate tetrahedra in garnet:

$$4\left(SiO_3 + Mg\right) \;\rightarrow\; 3(SiO_4) + Si + 4Mg$$

That is, in $Mg_4Si_4O_{12}$ three of the silicon ions are inside SiO_4 tetrahedra ($3\ SiO_4 = Si_3O_{12}$), and the other silicon and the four magnesium make up the five metal ions occupying spaces between the tetrahedra.

There is a similar range of compositions for garnet as for pyroxene. Also, pyroxene in the Earth's crust and mantle is often mixed with Al_2O_3 (corundum). One Mg^{2+} ion in the garnet can then be replaced by Al^{3+} from the corundum. This produces a charge imbalance which can only be compensated if one Si^{4+} ion is also replaced by Al^{3+}, giving aluminous garnet, $Mg_3Al_2Si_3O_{12}$ (pyrope):

$$Mg_4Si_4O_{12} + Al_2O_3 \;\rightarrow\; Mg_3Al_2Si_3O_{12} \;+\; MgSiO_3$$
$$(\text{silicate garnet} + \text{corundum} \rightarrow \text{pyrope} + \text{pyroxene})$$

At the pressures and temperatures found in the upper mantle, aluminous garnet (pyrope) is also soluble in silicate garnet, producing aluminous silicate garnet (majorite, first synthesized in the lab by Ringwood and Major (1971)).

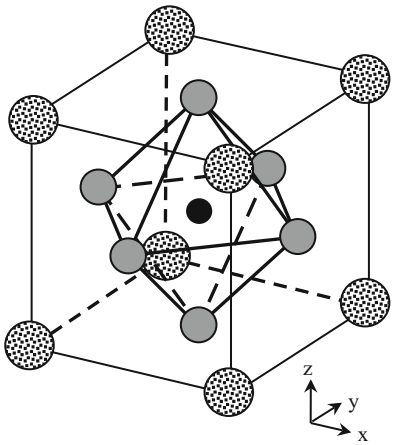

Fig. 7.14 Basic structural unit of a perovskite crystal. *Stippled circles*: Mg; *shaded circles*: O; *black circle*: Si

The crystal structure of corundum consists of alternating layers of oxygen and aluminum. The oxygen forms an HCP lattice, and the aluminum occupies distorted octahedral sites between the layers of oxygen.

7.4.1.3 Silicate Ilmenite

Above 20 GPa, $Mg_4Si_4O_{12}$ garnet undergoes a phase transition to a form of $MgSiO_3$ with the same crystal structure as $FeTiO_3$ ilmenite. This form of $MgSiO_3$ is generally referred to as silicate ilmenite. The crystal structure is the same as corundum (Al_2O_3), described above, with the Mg^{2+} and Si^{4+} replacing the Al^{3+} in an ordered alternate fashion.

Silicate ilmenite exhibits the same continuous sequence of compositions from $MgSiO_3$ to $FeSiO_3$ as do pyroxene and garnet.

7.4.1.4 Perovskite

Above 23 GPa, $MgSiO_3$ ilmenite undergoes a phase transition to a perovskite structure, $MgSiO_3$.

Figure 7.14 shows a basic structural unit of a perovskite crystal. The Mg^{2+} (stippled) and O^{4-} (shaded) ions form a face-centered cubic lattice with the Mg at the corners and the O at the centers of the faces. The Si^{4+} ion (black) is located at the center of the cube. Figure 7.14 shows that the oxygen ions form an octahedron with the silicon at its center.

When we abut other cubes against this one, they all share adjoining faces and corners. Consequently, each O ion is shared between two cubes and each Mg ion is shared between eight cubes. The perovskite crystal thus consists of linked SiO_6 octahedra in which each octahedron shares all six corner oxygen ions with its neighboring octahedra, and the magnesium ions occupy the spaces between the SiO_6 octahedra.

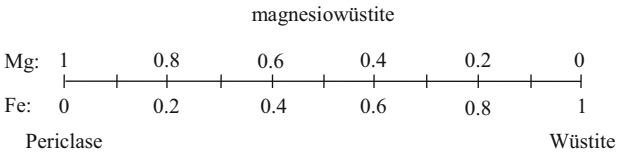

Fig. 7.15 Periclase–wüstite series

Now imagine an infinitely repeating sequence of such cubes in all directions to form a perovskite crystal. Some thought will show that every octahedron has a Mg ion to its lower right (as viewed in Fig. 7.14), and that this statement accounts for all the Mg ions; thus there is one Mg ion for every SiO_6 octahedron in the crystal. Also, if we imagine walking along each of the x, *y*, and *z* axes indicated in Fig. 7.14, then starting from any silicon ion, along each axis we have one Si, one O, one Si, one O, etc. There are three axes, so there are three O ions for each Si in the crystal. The chemical symbol for silicate perovskite is thus $MgSiO_3$, despite the fact that the basic building block is an SiO_6 octahedron.

In similar fashion to olivine and pyroxene, perovskite forms a continuous series in which some Mg ions are replaced by Fe, giving $(Mg_{(1-x)}Fe_x)SiO_3$. This form of perovskite is probably the most abundant mineral in the entire Earth; it may make up more than 80 % by volume of the lower mantle.

Other minerals also have phases with perovskite structure at high pressure, such as $CaSiO_3$ and $CaMgSi_2O_6$ (diopside).

However, pure $FeSiO_3$ has no perovskite phase, because at high pressure it decomposes into stishovite and wüstite:

$$FeSiO_3 \rightarrow SiO_2\,(\text{stishovite}) + FeO(\text{wüstite}).$$

FeO (wüstite) and MgO (periclase) are two end-members of another continuous series, (Mg,Fe)O (magnesiowüstite), as indicated in Fig. 7.15.

Magnesiowüstite has the same crystal structure as table salt (NaCl). The larger, negative oxygen ions form a face-centered cubic close-packed lattice, with the smaller, positive Mg or Fe ions occupying the spaces. The Mg/Fe ions also form a face-centered cubic lattice.

7.4.1.5 Post-perovskite Phase

Two different groups in 2004 announced the discovery that, at a pressure of ~120 GPa, perovskite undergoes a phase transition to a new crystal structure referred to as *post-perovskite* (Murakami et al. 2004, Oganov and Ono 2004). As shown in Fig. 7.16, the structure consists of planes of SiO_6 octahedra stacked along the *b* axis with Mg^{2+} ions between the layers. Within each plane, the octahedra share O ions along their edges to form chains parallel to the *a* axis, and the chains are connected by shared apical O ions along the *c* axis. Because all O ions are shared, the chemical symbol is $MgSiO_3$, as for perovskite (Sect. 7.4.1.4). The Mg^{2+}

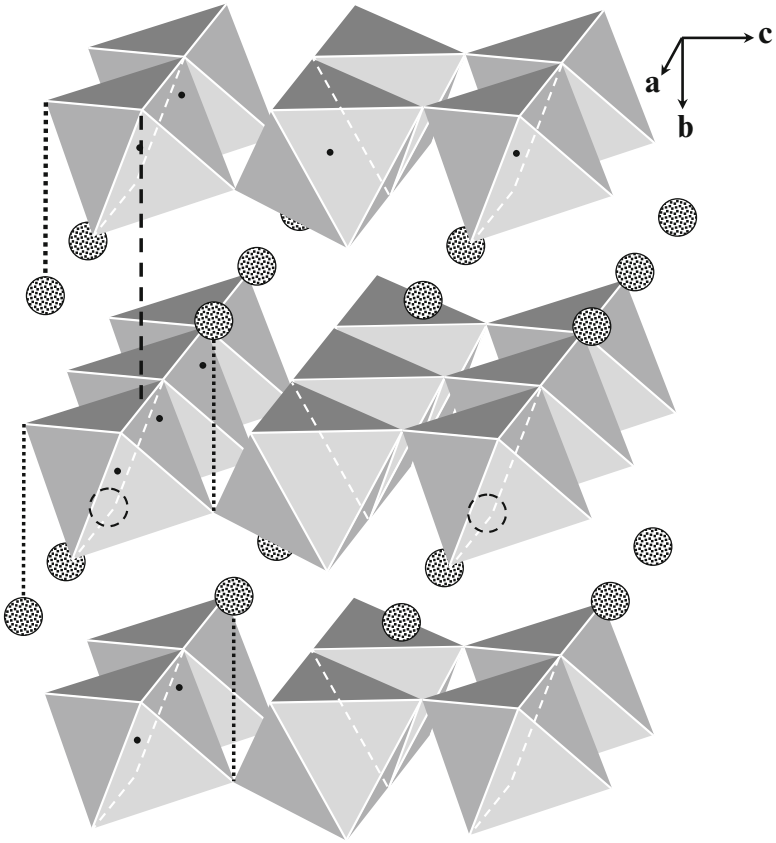

Fig. 7.16 Crystal structure of the post-perovskite phase of $MgSiO_3$ computed at 120 GPa pressure, derived from Figure 1 of Oganov & Ono (2004) and Figure 3 of Murakami et al. (2004). Stippled circles: Mg^{2+} ions (shown as a dashed circle if hidden behind an octahedron). Oxygen ions (not shown) are located at the corners of the octahedra, and each octahedron has a Si ion at its centre. The positions of some Si ions are indicated by black dots. The Mg^{2+} ions are located above or below apical O ions, as indicated by the four black dotted lines. Alternate planes of octahedra are displaced in the a-direction by half the width of an octahedron, as indicated by the black dashed line. Lines of Mg^{2+} ions are displaced in the a-direction by half the width of an octahedron relative to adjacent lines in both the b- and c-directions. Image drawn by W. J. F. Wilson from a handmade model

sites in post-perovskite are smaller than in perovskite, resulting in a volume reduction and corresponding density increase of 1.0–1.5 % (Hirose and Lay 2008).

7.4.1.6 Phase Diagrams for Pyroxene

Figure 7.17 shows a pressure-temperature phase diagram for pure $MgSiO_3$ for pressures and temperatures found in the Earth's mantle. As an example of phase transitions, the dashed, horizontal line illustrates the phase transitions from pyroxene to garnet to ilmenite to perovskite that would occur if pressure were to increase at a constant temperature of 2,000 °C.

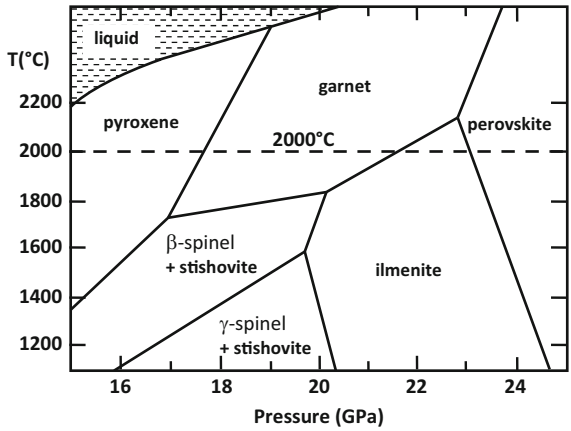

Fig. 7.17 Pressure-temperature phase diagram for $MgSiO_3$. Adapted from Anderson (1989), Fig. 16.4, p. 346, and appearing here with permission

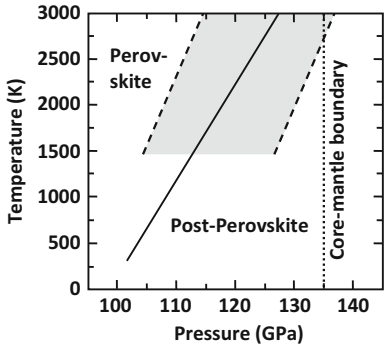

Fig. 7.18 Pressure-temperature phase diagram showing the computed perovskite-post-perovskite phase boundary for conditions in the lowermost ~800 km of the mantle. The position and slope of the phase boundary are somewhat uncertain, but the general appearance and strong, positive slope are as indicated. Two examples are shown, illustrating the range of computed slopes: *solid line*: Oganov and Ono (2004), Clapeyron slope 9.56 MPa/K; *dashed lines*: Catalli et al. (2009), Clapeyron slope 6.7 ± 0.5 MPa/K. Catalli et al. (2009) find a boundary width of ~20 GPa (*shaded area*) within which both phases are present

Figure 7.18 shows the perovskite-post-perovskite phase boundaries obtained by Oganov and Ono (2004) and Catalli et al. (2009) under lower-mantle conditions. The range in *Clapeyron slope* (the inverse of the slope in Fig. 7.18),

$$\frac{dP}{dT} = \frac{L}{T\Delta v} \tag{7.1}$$

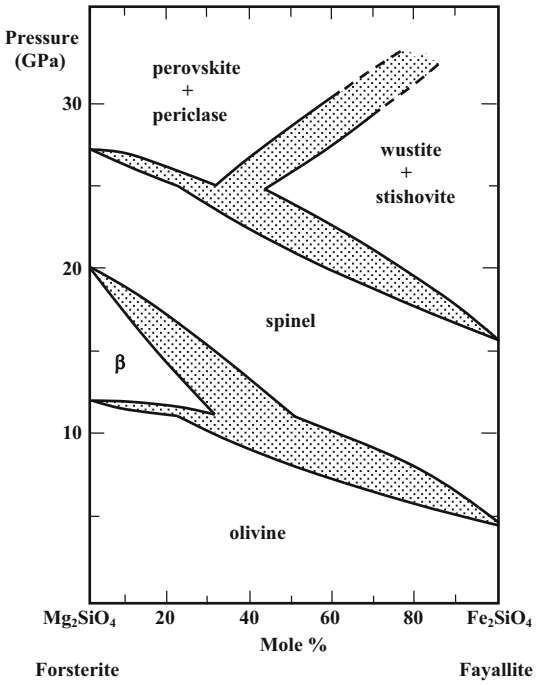

Fig. 7.19 Isothermal phase diagram at 1,000 °C for olivine (forsterite–fayalite system). From Bassett (1979), Fig. 6, p. 372, and reproduced here with permission

found for this transition is illustrated by the two boundaries shown: 9.56 MPa/K for Oganov and Ono (2004) and 6.7 ± 0.5 MPa/K for Catalli et al. (2009). In (7.1), L is the specific heat of transition (or latent heat), v is the specific volume (volume per unit mass, $v = 1/\rho$), and the equation assumes a sign convention in which heat input to the system is positive. If a sample of perovskite is compressed through the phase transition, then ρ increases and Δv is negative. Because the Clapeyron slope in Fig. 7.18 is positive, L in (7.1) must be negative; i.e., heat is released in the transition from perovskite to post-perovskite. The transition is therefore exothermic. In contrast, the ilmenite to perovskite transition (with a negative slope to the phase boundary in Fig. 7.17) is endothermic.

7.4.2 Phase Transitions of Olivine, Mg_2SiO_4

Figure 7.19 is an isothermal phase diagram of pressure versus iron fraction in the (Mg, Fe) part of olivine from 0 % (pure Mg_2SiO_4, forsterite) to 100 % (pure Fe_2SiO_4, fayalite), at a constant temperature of 1,000°C.

Olivine (also called α-phase) is the low-pressure phase. The crystal structure of olivine consists of isolated SiO_4 tetrahedra (not sharing oxygen atoms), with Mg or Fe in octahedral sites between the tetrahedra. The oxygen ions form an HCP lattice.

If the olivine is magnesium-rich, it undergoes a phase transition to β-phase (also called modified spinel) as pressure increases above about 20 GPa. Iron-rich olivine, however, has no β-phase and transforms directly into spinel.

β-Phase is denser than olivine, with a CCP (FCC) lattice of oxygen ions (see Sect. 7.2.1). The tetrahedra are in pairs that share an oxygen atom at one corner.

β-Phase (if magnesium-rich) or olivine (if iron-rich) transforms to a spinel structure at higher pressures. Spinel, also called γ-phase, has a CCP (FCC) lattice of oxygen ions with isolated tetrahedra, and is denser than either olivine or β-phase.

Many oxides crystallize with spinel structure, such $MgAl_2SiO_4$.

At higher pressures and temperatures, spinel decomposes into other minerals as shown in Fig. 7.19. It is interesting that, for the expected iron-to-magnesium ratio of about 90:10 in the mantle, both pyroxene and olivine produce perovskite at lower-mantle pressures.

7.5 Densities of Minerals

Table 7.4 lists the uncompressed densities (at 1 atmosphere pressure) of various minerals mentioned above.

7.6 Seismic Discontinuities in the Earth's Mantle

Figure 5.21 shows an empirical model of P- and S-wave speeds in the Earth's mantle, and the corresponding density profile, from Dziewonski and Anderson (1981). The three significant discontinuities in wave speed at depths of 220, 400, and 670 km below the Earth's surface all correspond to abrupt changes in density, and are believed to arise from phase changes in the solid rock with increasing depth (and therefore increasing pressure) in the mantle, as described below. The *Mohorovičić discontinuity*, or "*Moho*," marks the crust–mantle boundary and is believed to arise from a composition change from basaltic material in the crust to dunitic or peridotitic material in the upper mantle, rather than a phase change. Variations of depth or radius with latitude and longitude are not shown; e.g., the depth of the Moho varies from 5 km below oceanic crust to 35 km below continents and even 60 km or more below mountain ranges.

Table 7.4 Uncompressed densities of minerals (at 1 atm pressure) in kg/m^3

Olivine (Mg_2SiO_4) series		ρ	Pyroxene ($MgSiO_3$) series		ρ
Forsterite	Mg_2SiO_4	3,210	Enstatite	$MgSiO_3$	3,200
β-phase	Mg_2SiO_4	3,470	Garnet	$Mg_3Al_2Si_3O_{12}$	3,560
Spinel	Mg_2SiO_4	3,560	Ilmenite	$MgSiO_3$	3,800
Periclase	MgO	3,580	Perovskite	$MgSiO_3$	4,110
Stishovite	SiO_2	4,290			

7.7 Relationship of Phase Diagrams to Seismic Discontinuities

A model for the Earth's mantle is shown in Fig. 7.20 (Liu 1979), with the phase transitions described above plotted on a pressure scale (top horizontal axis) and also converted to depth into the Earth (bottom horizontal axis).

The density, ρ_o, plotted along the vertical axis in Fig. 7.20 is the uncompressed density, as in Table 7.4, not the actual density under pressure.

In this model, the 400 and 670 km seismic discontinuities are seen as arising from mineral phase transitions:

400 km discontinuity: olivine to β-phase

670 km discontinuity:

spinel to perovskite + periclase in the olivine component

and

garnet to ilmenite in the pyroxene/corundum component.

A small seismic discontinuity has sometimes been suspected between 400 and 650 km depth, and may result from the β-phase to spinel transition in the olivine component.

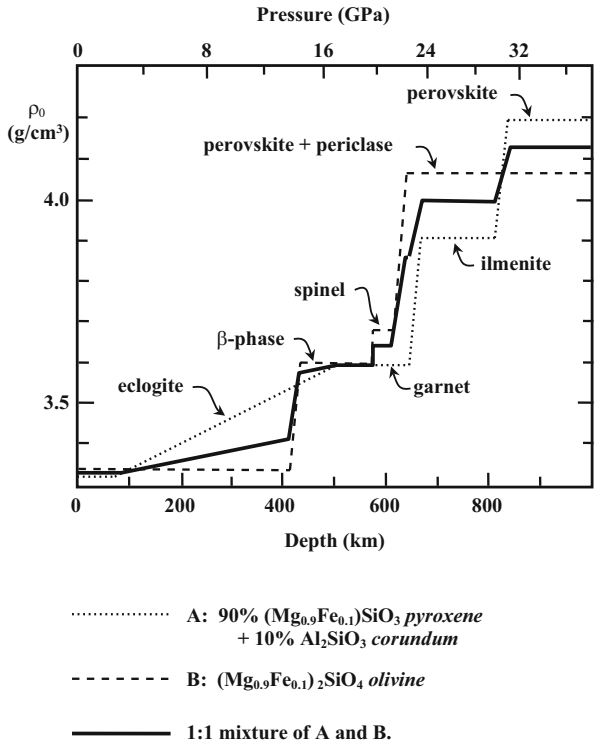

Fig. 7.20 Model of phase transitions in the mantle, with olivine, pyroxene, and corundum in the proportions given in the legend. From Liu (1979), Fig. 7, p. 195, with permission

Another small discontinuity below 670 km has also been suspected, and may be due to the transition from ilmenite to perovskite in the pyroxene/corundum component.

7.8 The Effect of Phase Boundaries on Mantle Convection

A phase boundary in a convecting region can have a significant effect on the convection, either intensifying it or inhibiting it.

Figure 7.21a illustrates two columns of rock in the mantle of a terrestrial planet, one convecting upward (left column) and the other downward (right column) through surrounding stationary rock. White indicates the less dense phase 1 and grey the more dense phase 2, with the phase boundary indicated by the dark line between them. As parcels of rock in the column rise or fall, the phase boundary within the column remains at a fixed depth (not necessarily the same depth as in the surrounding rock), and the rock changes phase as it passes through this boundary. Figure 7.21b shows a corresponding schematic phase diagram for the case where the transition from phase 1 to phase 2 is exothermic, so the slope of the phase boundary (solid line) is positive. The graph of temperature versus pressure for the surrounding rock (dashed line) crosses the phase boundary at point b. Pressure increases with increasing depth, so point b corresponds to a particular depth in the mantle (see Fig. 7.21a).

The effect of the phase boundary on the convection depends on the relative importance of three factors (Schubert et al. 1975): advection of temperature, latent heat, and thermal expansion. In the discussion below, we will consider these three factors separately, although in nature they occur together.

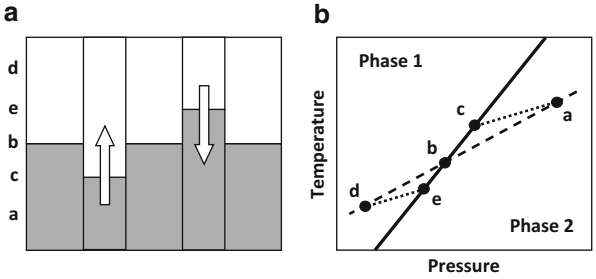

Fig. 7.21 Effect of phase boundaries on mantle convection. (**a**) Columns of rock convecting through surrounding stationary rock in the mantle in the presence of a phase boundary. *White*: Phase 1. *Grey*: Phase 2. The *arrows* show the direction of motion of each column. (**b**) Schematic phase diagram for the case of an exothermic phase change (heat is released) for a transition from the less dense phase 1 to the more dense phase 2. Greater pressure corresponds to greater depth. *Solid line*: Phase boundary. *Dashed line*: Temperature (T) versus pressure (P) in the surrounding rock. *Dotted line* (**a**–**c**): T versus P for a parcel of rock in the ascending column. *Dotted line* (**d**–**e**): T versus P for a parcel of rock in the descending column. Letters are explained in the text

1. Advection of temperature. Consider a parcel of rock in the rising column, located in phase 2 at some point, a, below the phase boundary. For purposes of discussion, we will assume that the parcel and the surrounding rock have the same temperature at point a. Heat takes time to diffuse between the parcel and its surroundings, so as the parcel rises into cooler rock it finds itself hotter than its surroundings. The parcel reaches the phase boundary (and changes phase) at point c. Because the phase boundary has a positive slope, point c is at a higher pressure (greater depth) than point b. The rock between points c and b in the rising column (see Fig. 7.21a) is then less dense than its surroundings and its buoyancy intensifies the convection. A parcel in phase 1, descending from point d, finds itself cooler than the surrounding rock and changes phase at point e, at a lower temperature and pressure and therefore smaller depth than in the surrounding rock. The descending rock between points e and b therefore finds itself denser than its surroundings, and its negative buoyancy also intensifies the convection. It is left as an exercise for the reader to show that, if the phase change from phase 1 to phase 2 is endothermic (negative slope to the phase boundary), then the displacements of the phase boundary are opposite to those in Fig. 7.21a, and advection of temperature inhibits convection.

2. Latent heat. If the transition is exothermic from phase 1 to phase 2, then it is endothermic from phase 2 to phase 1. The phase change at point c then cools the rising parcel, and it slides downward along the phase boundary in Fig. 7.21b as the transition proceeds. Conversely, the descending parcel is heated by the exothermic transition, and slides upward along the phase boundary. In both cases, the release or absorption of latent heat acts to oppose the effect of advection of temperature, inhibiting convection. It is left as an exercise for the reader to show that, if the transition from phase 1 to phase 2 is endothermic (negative slope), the release or absorption of latent heat adds to the effect of advection of temperature (which is to inhibit convection), thus further inhibiting convection. The release or absorption of latent heat therefore acts to inhibit convection for all cases.

3. Thermal expansion. If the transition from phase 1 to phase 2 is exothermic, then in the ascending (descending) parcel, the decrease (increase) in temperature resulting from the absorption (release) of latent heat causes the parcel to contract and become denser (expand and become less dense), inhibiting convection in both cases. If the transition from phase 1 to phase 2 is endothermic, then convection is intensified. Note that the effect in point 3 is opposite to that in point 1, above.

Thus, whether the transition from phase 1 to phase 2 is exothermic or endothermic, one factor amplifies convection and the other two inhibit it. Whether convection is amplified or inhibited in the combined effect can be determined only from quantitative stability computations; but as a rule exothermic phase transitions amplify convection and endothermic transitions inhibit it (Breuer et al. 1996).

7.9 The Core–Mantle Boundary and the D″ Layer

The D″ layer, shown schematically in Fig. 7.22, is a region about 200–300 km thick observed at the base of the lower mantle, in contact with the core. Its upper boundary is defined by a discontinuity in which in the S-wave velocity, v_S, increases by 2–3 % from the lower mantle to the D″ layer (Catalli et al. 2009; see also Hirose and Lay 2008 for a review of the D″ layer). Any discontinuity in the P-wave velocity, v_P, however, is generally much smaller or absent.

Globally, the depth of the S-wave discontinuity (and therefore the thickness of the D″ layer) varies laterally by 40–50 km, and the discontinuity may even disappear in places. Within the D″ layer, S-waves show an anisotropy in which the velocities, v_{SH}, of horizontally-polarized S-waves (SH waves) are ~1 % greater than v_{SV}, the velocities of vertically-polarized S-waves (SV waves) over most of the D″ layer (Panning and Romanowicz 2004). However, the anisotropy is reversed ($v_{SV} > v_{SH}$) at the base of two broad low-velocity regions, often called *superplumes*, in the mantle below the Pacific Ocean and Africa.

Seismic studies of the D″ layer indicate a heterogeneous composition, both radially and laterally, perhaps due to ancient material left over from mantle differentiation, subducted oceanic lithospheric slabs reaching the base of the mantle, and core-mantle chemical reactions, and also a possible narrow thermal boundary layer in contact with the core where heat flow is by conduction rather than convection (Hirose and Lay 2008). However, a more thorough understanding of

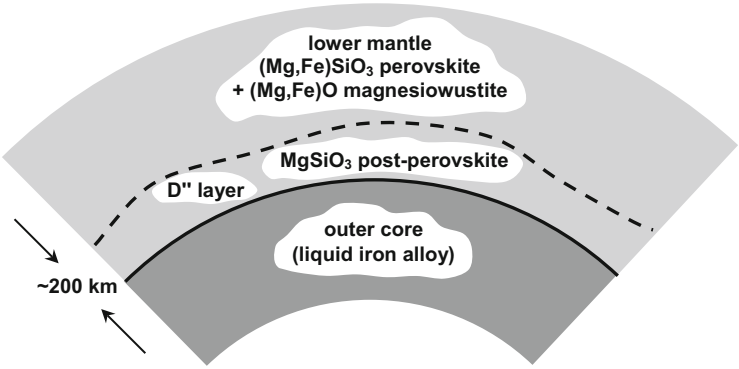

Fig. 7.22 The D″ layer, a layer of heterogeneous composition at the base of the upper mantle

many characteristics, particularly the S-wave anisotropy, had to await the discovery of the post-perovskite phase of pyroxene in 2004 (Sect. 7.4.1.5). Some points regarding this phase transition are (see Hirose and Lay 2008):

1. Computations and experiments at temperatures and pressures characteristic of the core-mantle boundary using laser-heated diamond-anvil cells show that the phase change creates a 1.4–4 % increase in v_S but only ±0.5 % change in v_P. Velocity changes of <0.5 % are difficult to measure, so both of these results are consistent with the observations mentioned above.

2. The large, positive Clapeyron slope in Fig. 7.18 means that the phase transition will occur at a shallower depth for cooler, subducting material and deeper for warmer, rising material in plumes (Fig. 7.21), contributing to the lateral depth variations described above.

3. The stacked plane structure of post-perovskite provides a natural explanation for the S-wave anisotropy described above. If there were large-scale lateral flow in some parts of the D″ layer and vertical flow in others, then the stacked planes would act as slip planes, and the crystals would tend to align with their slip planes parallel to the flow. They would also be more compressible along an axis perpendicular to the planes than within the planes. The S-wave velocity is given by

$$v_S = \sqrt{\frac{\mu}{\rho}} \tag{7.2}$$

   where μ is the rigidity of the material and ρ is the density, so S waves whose polarization axes lie in the crystal planes (where the rigidity is greater) would travel faster than those polarized perpendicular to the planes. The horizontal and vertical anisotropies then suggest that the D″ layer forms a boundary layer for mantle convection, with subducting material entering, plumes leaving, and lateral flow between.

4. Seismic observations often show an anticorrelation between S-wave velocity, v_S, and *bulk-sound-wave velocity*, v_C, in the D″ layer. The bulk wave velocity is given by

$$v_C = \sqrt{\frac{K_S}{\rho}} = \sqrt{v_P^2 - \frac{4}{3}v_S^2} \tag{7.3}$$

   where K_S is the bulk modulus. Calculations show that v_C is larger and v_S is smaller in post-perovskite than in perovskite, accounting at least in part for this anticorrelation.

In Fig. 7.18, the positive slope of the phase boundary means that the phase boundary contacts the core boundary at some temperature (~4,750 K in Fig. 7.18, but this temperature is uncertain due to uncertainties in the position and slope of the boundary). The Earth's interior was hotter when it first formed, so there would have been no post-perovskite phase. This may have a significant effect on the Earth's evolution, because stability calculations indicate that convection is amplified by a perovskite-post-perovskite phase boundary (see Sect. 7.8). This amplification does not occur if the post-perovskite phase is absent. Therefore, there may have been a relatively sudden increase in mantle convection and the rate of heat flow at some point, perhaps fairly long after the Earth formed.

There could also be implications for mantle convection in smaller planets such as Mercury and Mars, in which pressures are too low for post-perovskite to appear, and more massive extrasolar planets (super-Earths), where the post-perovskite layer would be much more extensive.

In Chap. 8, we will apply this information to material collected from our closest external body, the Moon; and, in Chap. 9, to Mercury, Venus and Mars.

References

Anderson, D.L.: Theory of the Earth. Blackwell, Oxford (1989)

Bassett, W.A.: The diamond cell and the nature of the earth's mantle. Annu. Rev. Earth Planet. Sci. **7**, 357–384 (1979)

Breuer, D., Zhou, H., Yuen, D.A., Spohn, T.: Phase transitions in the Martian mantle: implications for the planet's volcanic evolution. J. Geophys. Res. **101**, 7531–7542 (1996)

Catalli, K., Shim, S.-H., Prakapenka, V.: Thickness and Clapeyron slope of the post-perovskite boundary. Nature **462**, 782–785 (2009)

Dziewonski, A.M., Anderson, D.L.: Preliminary reference earth model. Phys. Earth Planet.In. **25**, 297–356 (1981)

Hirose, K., Lay, T.: Discovery of post-perovskite and new views on the Core–Mantle boundary region. Elements **4**(3), 183–189 (2008)

Liu, L.G.: Phase transformations and the construction of the Deep Mantle. In: McElhinny, M.W. (ed.) The Earth: Its Origin, Structure and Evolution, pp. 117–202. Academic Press, London (1979)

Murakami, M., Hirose, K., Kawamura, K., Sata, N., Ohishi, Y.: Post-perovskite phase transition in $MgSiO_3$. Science. **304**, 855–858 (2004)

Oganov, A.R., Ono, S.: Theoretical and experimental evidence for a post-perovskite phase of $MgSiO_3$ in Earth's D″ layer. Nature **430**, 445–448 (2004)

Panning, M., Romanowicz, B.: Inferences on flow at the base of Earth's mantle based on seismic anisotropy. Science **302**, 351–353 (2004)

Ringwood, A.E., Major, A.: Synthesis of majorite and other high pressure garnets and perovskites. Earth Planet. Sci. Lett. **12**, 411–418 (1971)

Schubert, G., Yuen, D.A., Turcotte, D.L.: Role of phase transitions in a dynamic mantle. Geophys. J. Roy Astron Soc **42**, 705–735 (1975)